Journal of Power Sources 196 (2011) 1392–1398

Contents lists available at ScienceDirect

Journal of Power Sources

journal homepage: www.elsevier.com/locate/jpowsour

Modification of the $Li_xV_2O_5$ phase diagram by incorporation of chromium oxide

J.P. Pereira-Ramos [a,*], P. Soudan [a], R. Baddour-Hadjean [a], S. Bach [a,b]

[a] Institut de Chimie et des Matériaux Paris Est, ICMPE/GESMAT, UMR 7182 CNRS-Université Paris Est Créteil, CNRS 2 rue Henri Dunant, 94320 Thiais, France
[b] Université d'Evry Val d'Essonne, Bd F. Mitterrand, Departement Materiaux, 91025 Evry Cédex, France

ARTICLE INFO

Article history:
Received 12 May 2010
Received in revised form 24 August 2010
Accepted 25 August 2010

Keywords:
Chromium–vanadium mixed oxide
Rechargeable cathode
Li batteries
Single phase behaviour

ABSTRACT

The structural behaviour of the sol–gel chromium–vanadium mixed oxide $Cr_{0.11}V_2O_{5.16}$ is investigated as electrochemical lithium insertion proceeds. Electrochemically reduced electrodes are examined by XRD over the large Li composition range $0 < x \leq 2$ in $Li_xCr_{0.11}V_2O_{5.16}$. New fingerprints of lithiated phases are obtained in comparison with available data in the Li–V_2O_5 system. It is shown that lithiation produces an ε-related phase over a wide composition range $0.18 \leq x \leq 2$ whose interlayer distance linearly increases with x which strongly contrasts with the successive appearance of the (α/ε), (ε/δ), and (δ/γ) wide biphasic regions for the $Li_xV_2O_5$ system. The existence of shorts chains of CrO_6 octahedra perpendicular to V_2O_5 layers increases the three-dimensional character of the host lattice impeding then too strong deformations to occur. These limited structural changes resulting in a single phase behaviour are discussed in relation with the original and promising electrochemical properties of the sol–gel mixed oxide $Cr_{0.11}V_2O_{5.16}$.

1. Introduction

While V_2O_5 was one of the earliest oxides studied as lithium intercalation compounds [1], vanadium pentoxide is still the objective of many works as positive electrode material in secondary lithium batteries. Its open structure (orthorhombic symmetry) combined with a theoretical high specific capacity of 450 mAh g^{-1} has prompted a great effort to consider closely related forms like V_2O_5 xerogel [2,3] and high surface area aerogels [4,5] either to modify the discharge–charge profile, or to enhance the lithium insertion capacity and to improve the rate capability. Nanosizing effect has been also evaluated by many groups to optimize the electrochemical properties especially by shortening the lithium diffusion pathway [6–8]. Another way can be applied by using derivative forms of the orthorhombic V_2O_5. For instance, divalent cations were incorporated in the V_2O_5 framework to give $M_{0.16}V_2O_5$ mixed oxides with M = Ni^{2+}, Cu^{2+}, Co^{2+} [9,10] and Ba^{2+} [11] respectively prepared by a solution technique and a sol–gel process. These cathode materials were evaluated without any improvement in comparison with that known for the V_2O_5 parent oxide. Ten years ago, our group reported the sol–gel chemistry offers a new approach to get new orthorhombic $M_{0.11}V_2O_{5.16}$ mixed oxides where M is a trivalent metallic ion (M = Al^{3+}, Fe^{3+}, Cr^{3+}) [12–14] with a structure very close to that of the parent oxide but characterized by original and improved electrochemical properties. Among them, the chromium–vanadium mixed oxide was reported to be the most attractive electrode material with a specific capacity of 260 mAh g^{-1} stable over 20 cycles at C/10 in the 3.8–2 V potential range. This corresponds to a gain in the range 10–15% in comparison with the pristine oxide. However the most striking result consisted in the significant modification of the discharge–charge profile compared to that of the V_2O_5 parent oxide. In fact, the voltage–composition curve of V_2O_5 is well-known to account for the $Li_xV_2O_5$ phase diagram reported in [15–18]. Depending on the amount of Li ions (x) intercalated in V_2O_5 according to the electrochemical reaction: $V_2O_5 + x + xLi^+ \Leftrightarrow Li_xV_2O_5$, several structural modifications take place for the bulk material. The α-, ε-, and δ-$Li_xV_2O_5$ phases were identified from the above reaction in the $0 < x \leq 1$ composition range. The α-$Li_xV_2O_5$ phase occurs with $x < 0.1$. The ε-$Li_xV_2O_5$ phase exists in the range $0.3 < x < 0.7$ and the δ-$Li_xV_2O_5$ phase appears with x between 0.9 and 1. The lithium content corresponding to the limiting composition of the three solid solutions differs slightly from one report to another. All these phase transitions are fully reversible in this composition range and the structure of the pristine V_2O_5 phase is recovered upon deintercalation. But, if more than 1 lithium ion is accommodated, then significant permanent structural changes occur giving the γ phase leading to a new metastable γ′ variety of V_2O_5 after Li deintercalation [17,18]. The voltage plateaus at 3.4 V, 3.2 V and 2.3 V of the equilibrium potential curve E vs. x are ascribed to the successive (α/ε), (ε/δ), and (δ/γ) biphasic regions respectively [17,18].

Therefore in a first approach, the sloped discharge curves observed for the $Li_xCr_{0.11}V_2O_{5.16}$ system in the same potential

* Corresponding author. Tel.: +33 1 49 78 12 79; fax: +33 1 49 78 11 95.
E-mail address: pereira@icmpe.cnrs.fr (J.P. Pereira-Ramos).

0378-7753/$ – see front matter © 2010 Elsevier B.V. All rights reserved.
doi:10.1016/j.jpowsour.2010.08.080

range 3.8–2 V can suggest more limited structural changes which could explain the better cycle life of the mixed oxide [14].

In the present paper, we report a detailed view of the electrochemical behaviour of this electrode material and investigate the structural effect of electrochemical Li insertion on the host lattice of the sol–gel mixed oxide $Cr_{0.11}V_2O_{5.16}$ over the potential range 3.8–2 V in liquid electrolyte. This approach should provide useful information to understand the new electrochemical behaviour found for this chromium oxide-doped V_2O_5 material and to answer the question of fundamental importance on how to modify the phase diagram of a host lattice upon Li insertion.

2. Experimental

The basic material, the V_2O_5 gel with formula V_2O_5, nH_2O, is prepared by spontaneous polycondensation of decavanadic acid [19]. The sol–gel process is based on the acidification of a metavanadate solution by passing through an ion exchange resin. Gelation is observed when the vanadium concentration is higher than 0.1 M. The red viscous gel deposited on a glass plate loses most of its water readily at room temperature, leading to a thin film of V_2O_5, xerogel (VXG) with the following schematic formula [2]: $(V_2O_{5.16})^{0.33-}0.33H_3O^+xH_2O$ ($x \approx 1.3$). VXG is made of negatively charged ribbons between which are located hydronium ions (ca. 0.33 per mole of oxide). The latter ensure the global electroneutrality and constitute the ionic exchange capacity of the xerogel. The $0.33H_3O^+$ ions contained per mole of VXG are quantitatively exchanged with Cr^{3+} ions by soaking the film in a 0.1 M $Cr(NO_3)_3$ aqueous solution. A further heat treatment of the exchanged VXG at 520 °C for 2 h in air gives rise to the formation of platelets of a few micrometers thick of the mixed oxide $Cr_{0.11}V_2O_{5.16}$. The final material consists of thin platelets which are ground for XRD and electrochemical experiments. The cation contents have been determined by atomic emission spectroscopy (induced coupled plasma). The oxidation states of vanadium and chromium have been deduced from chemical redox titration. The results lead to the formula $Cr_{0.11}V_2O_{5.16}$ in which the oxidation states of vanadium and chromium are 5 and 3 respectively.

The X-ray powder diffraction experiments were performed with a Siemens D5000 diffractometer equipped with Co K_α radiation (λ = 1.7889 Å) and a back graphite monochromator, or with a Inel diffractometer using the Cu K_α radiation (λ = 1.5406 Å).

High purity propylene carbonate (PC) was obtained from Fluka and used as received. Anhydrous lithium perchlorate was dried under vacuum at 200 °C for 12 h. The electrolyte (1 M $LiClO_4$/PC) was prepared under a purified argon atmosphere. We used conventional three electrode cells under argon atmosphere. The composite working electrode consists of a mixture of oxide (80% by weight) with a binder agent (PTFE, 5%), graphite (7.5%) and acetylene black (7.5%) as electronic conductors pressed under 5×10^3 kg cm^{-2} on a stainless steel grid. Reference and counter electrodes were made of lithium wires in separate compartments filled up with electrolyte. Electrochemical measurements were made with a potentiostat PAR 273 A coupled with an IBM 386 computer. Electrochemical lithiation of electrodes was performed at C/20 rate and equilibrium was considered to be reached when the open circuit voltage remained stable (±1 mV) for 12 h.

3. Results and discussion

The X-ray diffraction pattern in reflection geometry of the chromium intercalated xerogel is shown in Fig. 1. This compound exhibits a highly preferred *00l* orientation corresponding to the stacking of the ribbons along the *c* direction. The corresponding inter-ribbons distance is 14.27 Å with two water layers as deduced

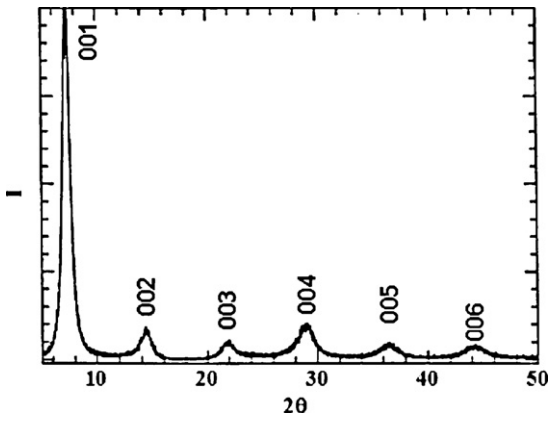

Fig. 1. XRD pattern of the chromium intercalated xerogel $Cr_{0.11}V_2O_{5.16}$, $2.34H_2O$ (λCo K_α = 1.7889 Å).

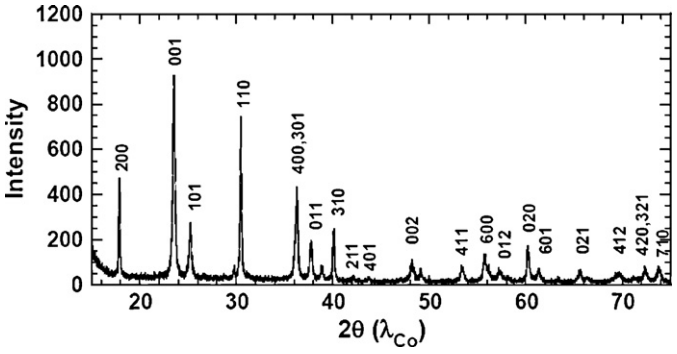

Fig. 2. XRD pattern of the previously ground mixed oxide $Cr_{0.11}V_2O_{5.16}$ (λCo K_α = 1.7889 Å).

from thermogravimetric analysis. Finally, the chemical composition of the chromium intercalated xerogel is $Cr_{0.11}V_2O_{5.16}$, $2.34H_2O$. The heat treatment of this xerogel at 520 °C in air for 2 h gives rise to the well crystallized compound $Cr_{0.11}V_2O_{5.16}$. The corresponding XRD pattern (Fig. 2) shows well defined diffraction lines all indexed on the basis of an orthorhombic cell (*Pmmn* space group) with the following unit cell parameters: a = 11.485 Å; b = 3.564 Å; c = 4.382 Å. These values are very close to those of the V_2O_5 parent oxide for which a, b and c are respectively 11.512 Å, 3.564 Å and 4.371 Å. Actually, a detailed XRD study of this compound has been performed in comparison with that of V_2O_5 [20]. The structure has been refined with a Rietveld procedure and the atomic positions as well as values for inter-atomic distances and angles can be found in [20]. V_2O_5 has an orthorhombic layered structure built up from square pyramids [VO_5] sharing edges and corners, leading to V_2O_5 sheets linked together via weak vanadium–oxygen interactions parallel to the *c* direction (Fig. 3). The vanadium atom (4f sites) located within the

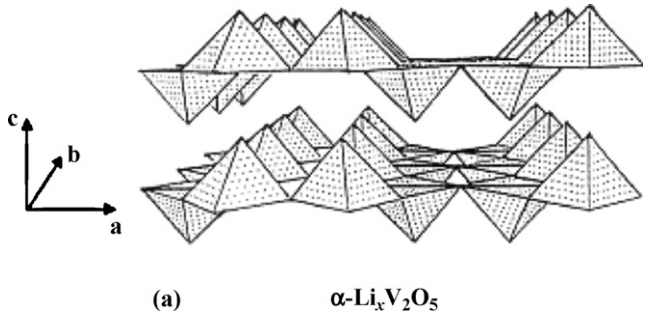

Fig. 3. Schematic view of the layered structure of V_2O_5.

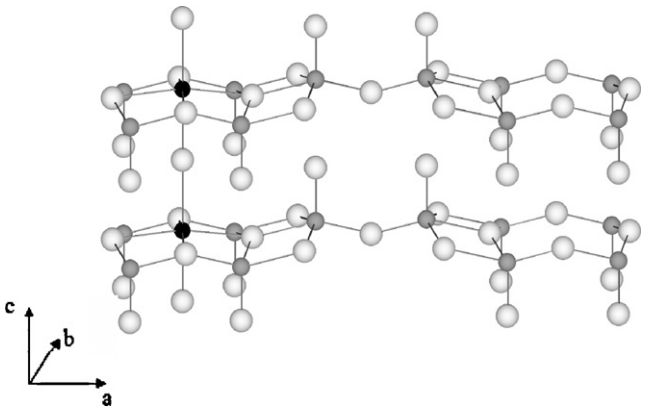

Fig. 4. Perspective view of $Cr_{0.11}V_2O_{5.16}$ structure: the Cr^{3+} ion which is located within the slabs of V_2O_5 has an octahedral environment. Grey circles, V^{5+} ions; white circles, O^{2-} ions; black circles, Cr^{3+} ions. Not all Cr^{3+} sites are occupied.

oxygenated coordination polyhedron VO_5 is shifted towards the plane formed by four oxygen atoms by a distance of 0.47 Å. In the case of the chromium–vanadium mixed oxide, the chromium ions are located in the 2b sites, almost at the centre of the average plane formed by four oxygen atoms of the V_2O_5 slab with two additional oxygen atoms located apart from the plane along the *c* direction in order to achieve an octahedral environment as illustrated in Fig. 4. According to the charge balance of the chemical formula, only 11% of the Cr^{3+} sites are occupied. Hence, the formation of short CrO_6 octahedra chains linking the V_2O_5 layers increases the three-dimensional character of the host lattice.

In a first approach, voltammetric measurements have been performed in the potential range 3.8 V/2 V at slow sweeping rate for the mixed oxide and the parent oxide. Fig. 5 reports the first two cycles for both materials. As expected for V_2O_5 [18], three reduction current peaks at 3.4 V, 3.2 V, 2.3 V are observed with the corresponding oxidation peaks respectively at 3.45 V, 3.3 V and 2.6 V. However, the electrochemical behaviour of V_2O_5 is not completely reversible as indicated by the emergence of a new redox system observed after the first intercalation process. Indeed, additional cathodic (3.6 V and 3.5 V) and anodic (3.65 V) peaks appear in the high potential region. The voltammetric fingerprint of the chromium–vanadium oxide strongly differs by a genuine reversible behaviour with reduction and oxidation curves which completely superimpose without any presence of the new system electroformed in the case of V_2O_5. It must be outlined also that the first two reduction current peaks (3.4 V and 3.2 V) and their related anodic peaks are exactly located at the same potential showing the highly reversible character of the Li insertion reaction in the 3.8–3 V range. A more detailed view of the electrochemical properties of the mixed oxide can be obtained from its discharge–charge curves reported at C/10 rate in the same cycling limits (Fig. 6). Three well defined and reversible insertion steps at 3.35 V, 3.15 V and 2.3 V allow to get a high faradaic yield of 2 F per mole of oxide corresponding to an initial specific capacity of 280 mAh g^{-1}, showing a increase by 10% in the capacity vs. the parent oxide. This discharge–charge profile, as well as the corresponding OCV curve reported in Fig. 7, contains both important and fundamental information. Indeed, looking more precisely at comparison of discharge–charge curves and OCV curves for the chromium mixed oxide $Cr_{0.11}V_2O_{5.16}$ and the parent oxide V_2O_5, a significant difference can be clearly seen. For V_2O_5 three well defined plateaus with constant voltage at 3.4 V, 3.2 V and 2.3 V correspond to the successive (α/ε), (ε/δ) and (δ/γ) biphasic regions [15–18] with a maximum Li uptake of 1.8 Li per mol of oxide. The high potential steps ($0 < x < 1$) lead to the reversible insertion of about 1 Li ion per mol of oxide, after which a sharp voltage drop appears up to the third plateau at 2.3 V ($1 < x \leq 1.8$) corresponding to the irreversible formation of the γ phase. Interestingly, the mixed oxide exhibits sloped curves vs. *x* for the first two insertion steps, i.e. for $x < 1$, a smooth potential decrease ensuring the transition before the third step also appearing as a sloped curve ($1 < x \leq 2$). This electrochemical finding supports the assumption of more limited structural changes.

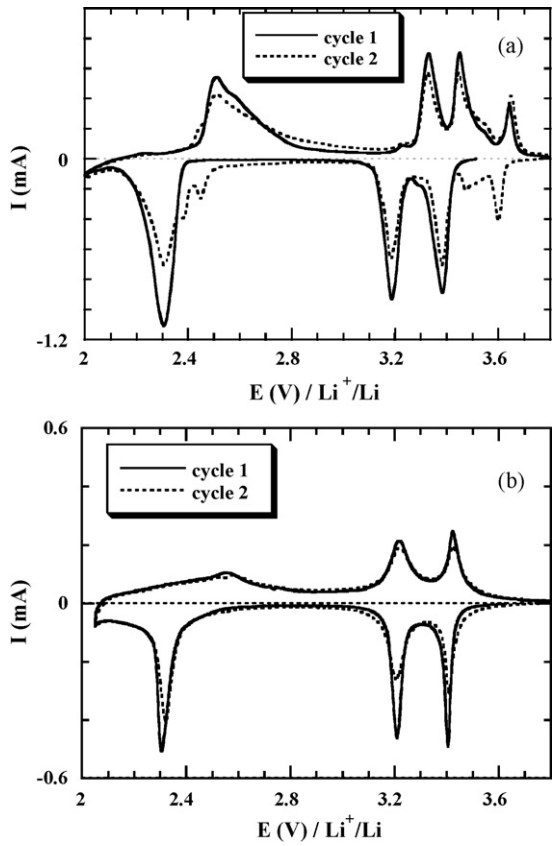

Fig. 5. Comparison of cyclic voltammetric curves for V_2O_5 (a) and $Cr_{0.11}V_2O_{5.16}$ (b) ($v = 10\ \mu V\ s^{-1}$).

XRD experiments have been performed for electrochemically lithiated samples $Li_xCr_{0.11}V_2O_{5.16}$ with $0 < x < 2$ in order to understand the effect of Li insertion into the host lattice of the chromium mixed oxide and to identify some expected differences with the

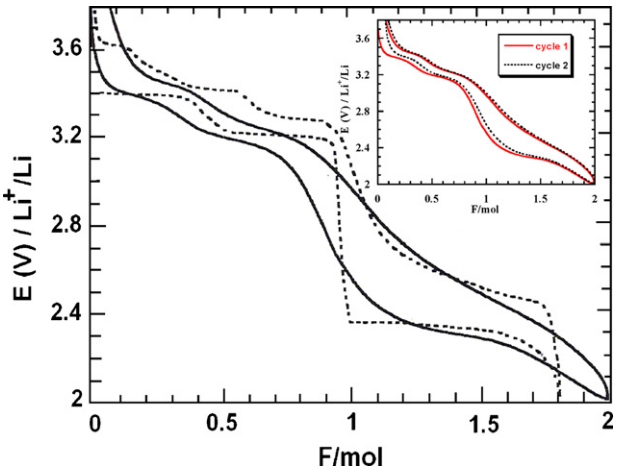

Fig. 6. Comparison of the first discharge–charge curves for $Cr_{0.11}V_2O_{5.16}$ and for V_2O_5 electrodes (dashed lines) in the 3.8–2 V potential range at C/10 rate; the first two cycles for the mixed oxide are shown in inset.

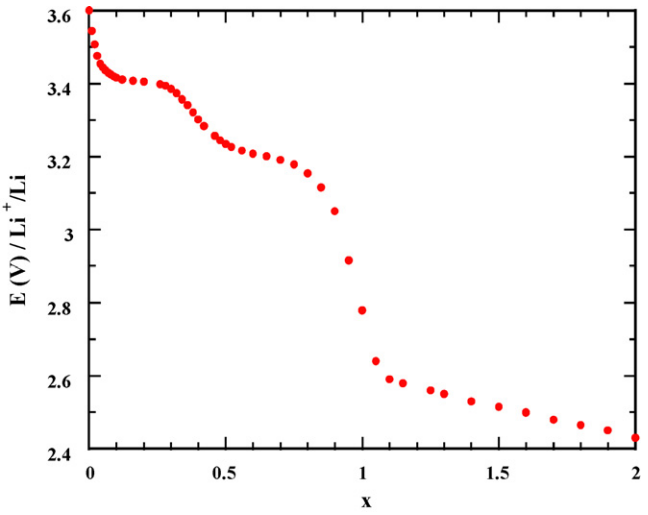

Fig. 7. OCV curve of a $Cr_{0.11}V_2O_{5.16}$ electrode as a function of x in $Li_xCr_{0.11}V_2O_{5.16}$.

$Li_xV_2O_5$ system. Fig. 8 displays the X-ray diffraction patterns of $Li_xCr_{0.11}V_2O_{5.16}$ electrodes for $0 \le x \le 0.93$. All the diffraction lines of the starting mixed oxide are maintained up to $x = 0.93$ without the emergence of a new phase and can be indexed in the orthorhombic symmetry (*Pmmn* space group). Only a shift of the diffraction lines is observed; the 200, 400 and 310 lines towards higher two theta values while all the other lines shift towards lower two theta values (Fig. 9). This indicates a continuous increase in the *c* parameter while the *a* parameter contracts with *x*. The trend observed for higher Li contents is illustrated in Fig. 10 for $1.2 \le x \le 2$: a shift towards lower two theta values occurs for the 001, 101 and

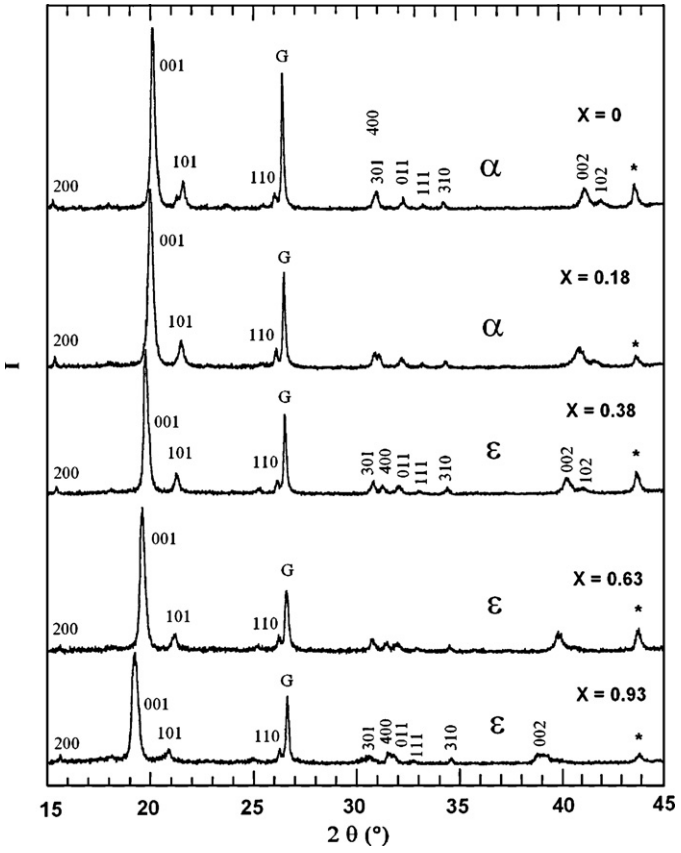

Fig. 8. X-ray diffraction patterns of $Li_xCr_{0.11}V_2O_{5.16}$ electrodes with $0 < x < 1$ (λCu K_α = 1.5406 Å); G: graphite; *: acetylene black.

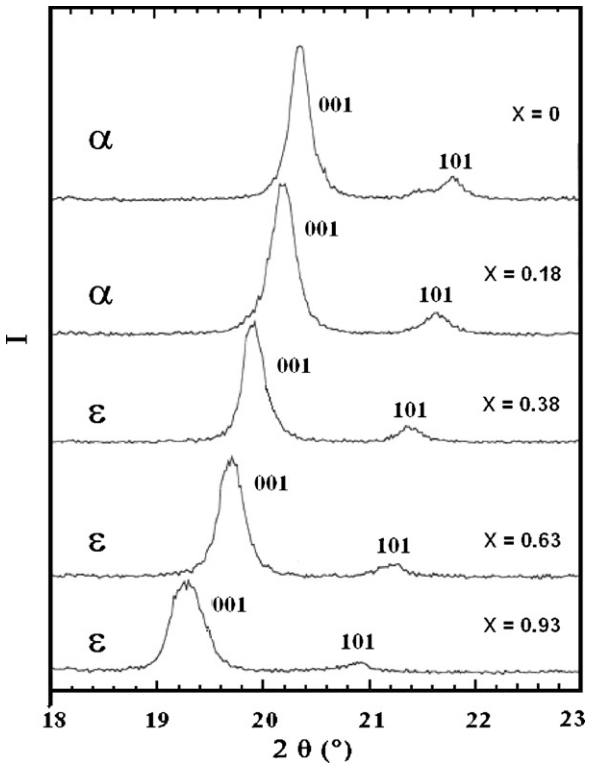

Fig. 9. Expanded view of the XRD patterns of $Li_xCr_{0.11}V_2O_{5.16}$ electrodes with $0 \le x \le 1$ in the 18–23° two theta range (λCu K_α = 1.5406 Å).

002 lines while the 400, 110, 301 and 310 lines do not practically move. This accounts for a new expansion in the *c* unit cell parameter while *a* is almost constant. These results highlight an original structural response which strongly differs from that known for the

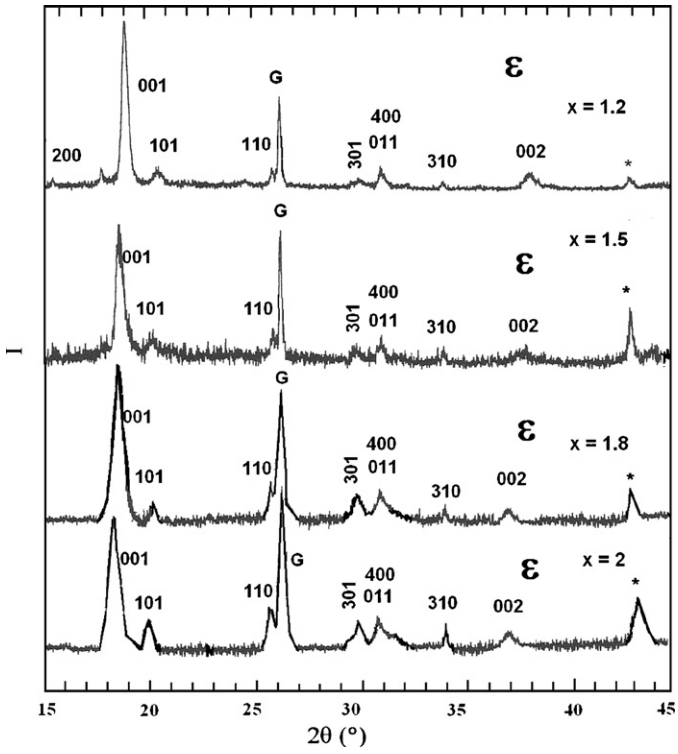

Fig. 10. X-ray diffraction patterns of $Li_xCr_{0.11}V_2O_{5.16}$ electrodes with $1.2 \le x < \le 2$ (λCu Kα = 1.5406 Å).

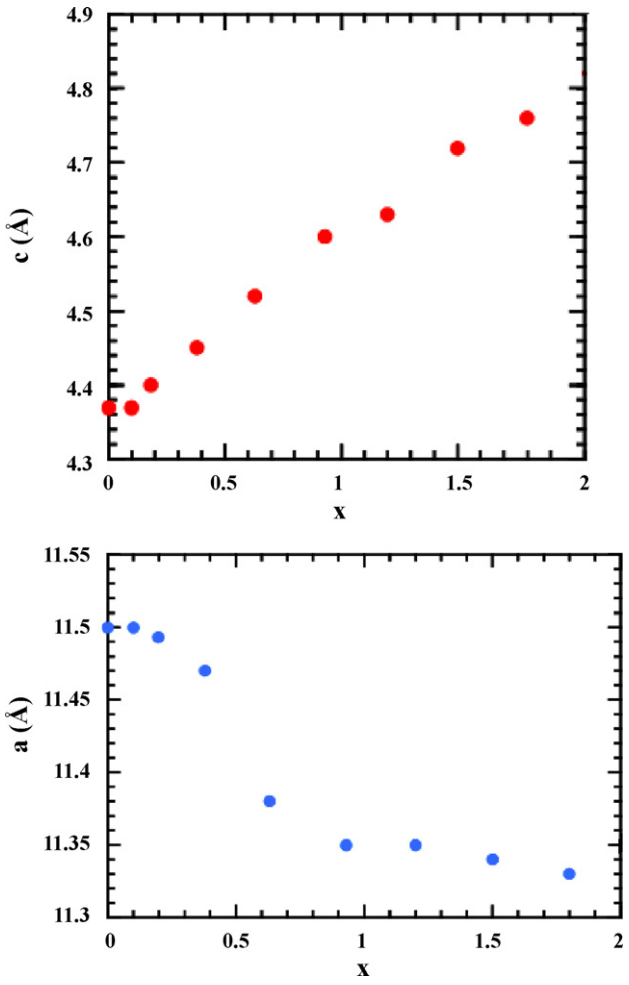

Fig. 11. Evolution of the unit cell parameters a and c as a function of x in $Li_xCr_{0.11}V_2O_{5.16}$.

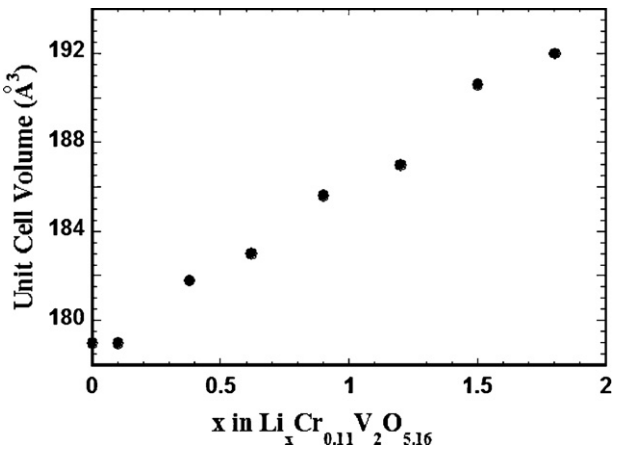

Fig. 12. Evolution of the unit cell volume vs. x in $Li_xCr_{0.11}V_2O_{5.16}$.

parent oxide insofar as the formation of the most distorted lithiated phases of the $Li_xV_2O_5$ phase diagram, namely the δ-LiV_2O_5 phase and the γ-LiV_2O_5 phase are never detected. In δ-LiV_2O_5 phase, the layers are much more puckered (space group *Amma*; $a = 11.23$ Å; $b = 3.61$ Å; $c = 9.9$ Å) and a shift of every second layer in the b direction is observed [21]. In the γ phase (space group *Pnma*, $a = 9.68$ Å; $b = 3.60$ Å; $c = 10.66$ Å), layer puckering is more pronounced than in the δ phase and the VO_5 pyramids alternate up and down individually instead of forming pairs as in δ phase [22]. The δ–γ structural transition then requires some chemical bonds are broken and the 180° rotation of some polyhedra. Hence, it comes out that the formation of the most distorted lithiated phases is suppressed in the case of the chromium–vanadium mixed oxide.

The evolution of the unit cell parameters a and c vs. lithium content which respectively accounts for the V–V distance within the V_2O_5 sheets and the interlayer distance is reported in Fig. 11. The interlayer distance is seen to continuously increase with Li content showing Li accommodation takes place between oxide layers; it expands from 4.37 Å to 4.60 Å for $x = 1$ against 4.95 Å for the expected δ-LiV_2O_5 phase.

A more limited expansion is observed in the $1 < x < 2$ composition range with a maximum value of 4.76 Å for $x = 1.8$ which is much less than the interlayer distance (5.34 Å) found in the γ-LiV_2O_5. These structural data demonstrate the original structural behaviour of the lithiated chromium mixed oxide which consists in a solid state solution well illustrated by the linear expansion of the unit cell volume vs. x (Fig. 12). Except for the first lithium ions ($x \leq 0.18$) where an α phase is observed, for $0.18 < x < 1$ all the diffraction lines can be indexed on the basis of an ε-related phase insofar as the ε phase in the $Li_xV_2O_5$ system has a typical value for the unit cell parameter c of 4.52 Å for ε-$Li_{0.52}V_2O_5$ [23]. The value of 4.68 Å reported for the chemically formed ε-LiV_2O_5 phase [24,25] makes pertinent the description of the $Li_xCr_{0.11}V_2O_{5.16}$ system as an ε-related phase with $0.18 < x \leq 1$. This ε-related phase still exists for $x > 1$ with a continuous interlayer expansion with x to reach 4.76 Å at $x = 1.8$, instead of the coexistence of δ-LiV_2O_5 and γ-LiV_2O_5 phases reported in the Li–V_2O_5 phase diagram [17,18]. Such structural characteristics have never been described as yet for the V_2O_5-based host lattice at room temperature. However closely related structural data can be found for reduced $Li_xFe_{0.11}V_2O_{5.16}$ electrodes [13]. In that case, the results indicated also a linear expansion in the c parameter for $0 < x < 0.8$, but rapidly the emergence of the δ-LiV_2O_5 phases from $x = 0.8$. In fact the formation of the δ- and γ-LiV_2O_5 phases was not avoided since the latter were clearly observed respectively for $x = 1$ and $x = 1.5$. Additional structural experiments should be performed to get conclusive remarks on the structural changes in the composition range $1 < x < 2$. This strong difference in the structural changes of the $Li_xFe_{0.11}V_2O_{5.16}$ and $Li_xCr_{0.11}V_2O_{5.16}$ systems could stem from the reduction of Fe^{3+} into Fe^{2+} while Cr^{3+} are not involved in the redox process allowing then to stabilize the structure over the composition range $0 < x < 2$.

The lack of the δ-LiV_2O_5 and the γ-LiV_2O_5 phases probably originates from the presence of the short chains of chromium oxide perpendicular to the V_2O_5 sheets impeding then the shift of one layer over two in the b direction as usually observed in the $Li_xV_2O_5$ system for $x \geq 0.9$. Because the δ phase cannot be formed, the γ phase whose formation is induced by further lithiation of the δ phase cannot be formed also.

An additional evidence for limited structural changes in $Cr_{0.11}V_2O_{5.16}$ is provided by its electrochemical fingerprint. Indeed the new current peaks and voltage plateaus located in the 3.5–3.6 V region for V_2O_5 (Figs. 5 and 6) due to the presence of the γ and γ′ phases [17,18] produced during the first reduction–oxidation process in the 3.8–2 V potential range do not appear which is in good accord with a single phase behaviour.

The chemical lithiation of $Cr_{0.11}V_2O_{5.16}$ by *n*-butyllithium in pentane has been performed in order to check the present structural finding in the case of electrochemically lithiated samples. Fig. 13 compares the XRD patterns of a chemically and electrochemically formed $Li_{\approx 1.5}Cr_{0.11}V_2O_{5.16}$ sample. In both cases, the same lithiated ε-related phase appears while the expected distorted γ-LiV_2O_5 phase is not detected. This confirms the presence of chromium oxide incorporated in the V_2O_5 framework avoids strong structural changes.

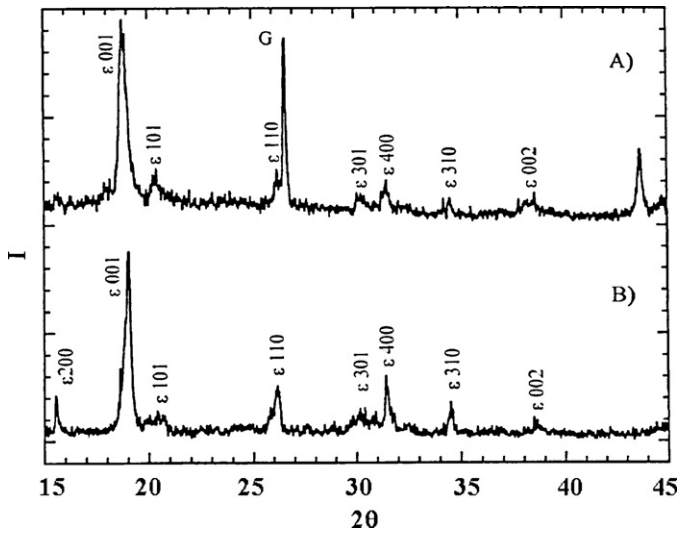

Fig. 13. Comparison of XRD patterns of an electrochemically (A) and chemically (B) lithiated $Li_{1.5}Cr_{0.11}V_2O_{5.16}$ sample (λCu K_α = 1.5406 Å).

Another important characteristic is the reversibility of the volume expansion of the host lattice after lithium extraction. The initial structure of $Cr_{0.11}V_2O_{5.16}$ (a = 11.50 Å; b = 3.51 Å; c = 4. 40 Å) is recovered after electrochemical oxidation of $Li_{1.5}Cr_{0.11}V_2O_{5.16}$ (a = 11.35 Å; b = 3.56 Å; c = 4. 70 Å) in good accord with the weakly modified structure obtained for the lithiated mixed oxide.

Discharge–charge cycling experiments performed between 3.8 V and 2 V show a high reversible behaviour since the capacity only decreases from 280 mAh g^{-1} to 260 mAh g^{-1} after 20 cycles at C/10 rate (Fig. 14). The main capacity loss is due to the first cycle during which a small amount of lithium ions seems to be trapped in the structure. From cycle 2, the capacity practically stabilizes over 20 cycles. XRD patterns for discharged electrodes after 5 cycles, 15 cycles and 30 cycles are reported in Fig. 15. Except a decrease in intensity with cycles, all the typical diffraction lines of the lithium rich ε-related phase $Li_{\approx 1.6-1.8}Cr_{0.11}V_2O_{5.16}$ are observed which ascertains the stabilizing role of chromium oxide is maintained during cycling operation to avoid the formation of more distorted phase like the δ-LiV_2O_5 and the γ-LiV_2O_5 phases. This result is consistent with the quasi stable capacity obtained for the chromium–vanadium mixed oxide. The small shoulder observed near the 001 line after 30 cycles could reveal the appearance of the 002 line of the δ phase suggesting that extended cycling could alter

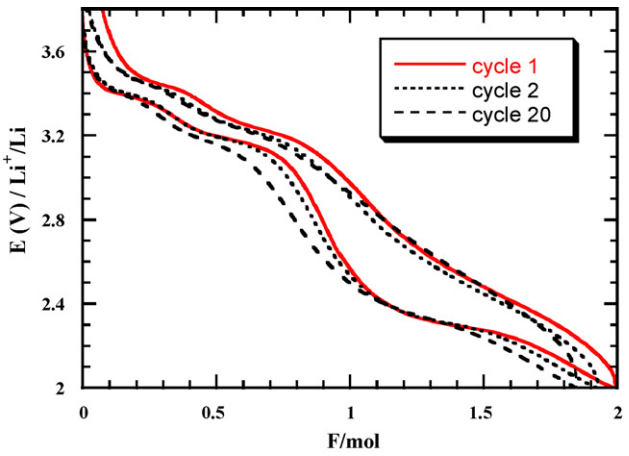

Fig. 14. Galvanostatic discharge–charge curves of $Cr_{0.11}V_2O_{5.16}$ cycled between 3.8 V and 2 V at C/10.

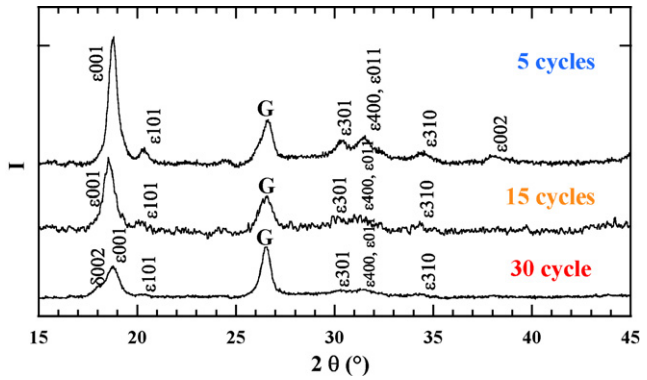

Fig. 15. XRD patterns of $Cr_{0.11}V_2O_{5.16}$ electrodes in the discharged state after 5 cycles, 15 cycles and 30 cycles at C/10 (λCu K_α = 1.5406 Å).

the stabilizing effect afforded by short chains of chromium oxide along the c axis. The decrease in XRD peaks could suggest a progressive electrochemical grinding due to the volume expansion of the host lattice (≈7%) as Li intercalation proceeds.

Recently, $Cr_{0.1}V_2O_{5.15}$ was prepared by an oxalic acid assisted sol–gel method followed by heat treatment at 400 °C [26]. In that case, the authors did not investigate the structural behaviour of the cathode material vs. the Li content, but simply reported the crystal structure of the material was destroyed after 50 cycles which was connected with potential profiles rapidly tuning to be slope-like instead of well defined redox steps. In the present work, a well defined discharge–charge profile is maintained during cycling in good accord with the expanded structure preserved upon cycling. Further work is in progress to investigate in details the structural answer of the chromium–vanadium mixed oxide during long term cycling experiments.

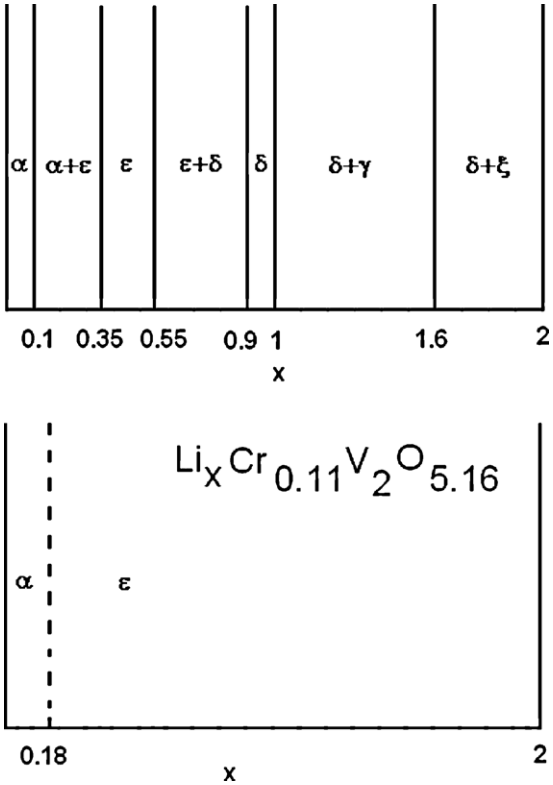

Fig. 16. Comparison of the phase diagrams vs. x for the $Li_xV_2O_5$ (from [18]) and $Li_xCr_{0.11}V_2O_{5.16}$ systems (this work).

The structural answer of the mixed oxide $Cr_{0.11}V_2O_{5.16}$ against Li insertion is the first example of the possible modification of the phase diagram for a Li intercalation compound over a wide composition range at room temperature. A similar effect has been outlined in the case of V_2O_5, not by doping the structure by additional cationic species, but with V_2O_5 platelets stacked over nanosized domains in the range 10–20 nm [27,28]. In the restricted composition range $0 < x < 1$, XRD and Raman experiments performed on electrochemically lithiated V_2O_5 thin films show an unexpected solid solution behaviour with lattice parameters changes very close to that reported here for $Cr_{0.11}V_2O_{5.16}$. In nanomaterials, the range of composition over which solid solutions exist is often more extensive because the strain associated with intercalation is better accommodated [29]. In all cases, OCV curves of $Li_xCr_{0.11}V_2O_{5.16}$ and $Li_xV_2O_5$ nanoplatelets are not dramatically changed in comparison with the microsized $Li_xV_2O_5$ system but clearly exhibit sloped curves vs. x instead of well defined voltage plateaus. This difference in the evolution of the equilibrium potential vs. x is consistent with the related structural response found for each material.

In other respects, it can be outlined that the role of chromium oxide chains inside the V_2O_5 host lattice at room temperature is similar to that induced by a temperature effect. Indeed, less severe structural rearrangements upon Li intercalation in V_2O_5 composite electrodes are suggested from electrochemical measurements at 100 °C with an extension of ε phase to $x = 1$ without formation of δ phase and no evidence for an irreversible conversion to the γ phase [30].

4. Conclusion

The electrochemical lithium insertion reaction into the sol–gel mixed oxide $Cr_{0.11}V_2O_{5.16}$ in liquid electrolyte has been investigated by X-ray diffraction. We show that the orthorhombic *Pmmn* symmetry of the pristine material is kept upon lithium intercalation in the $Li_xCr_{0.11}V_2O_{5.16}$ compounds over a wide lithium composition range ($0 < x \leq 2$). From the unit cell parameters variation as Li accommodation proceeds, the host lattice can be described on the basis of an ε-related phase characterized by a linear cell volume expansion of 7% in the voltage limits 3.8–2 V. Such a structural evolution contrasts with the $Li_xV_2O_5$ phase diagram which predicts the appearance of the successive phases α, ε, δ, γ. In a few words the presence of short chains of chromium oxide in V_2O_5 is seen to be responsible for a single phase behaviour which consists in a significant modification of the Li–V_2O_5 phase diagram (Fig. 16). As shown from the voltammetric and chronopotentiometric curves and from XRD data, these limited structural changes allow the complete recovery of the initial structure after the charge process while the γ' phase (the deintercalated distorted γ phase) is still detected in the case of V_2O_5. Such a moderate structural behaviour ensures a high electrochemical reversibility as outlined by the high and stable specific capacity of 260 mAh g^{-1} obtained over 20 cycles.

It comes out that besides nanosize and temperature effects, strong modification of the Li–V_2O_5 phase diagram can be induced through appropriate structural modifications of the host lattice. These modifications consist here in the existence of short CrO_6 octahedra chains linking the V_2O_5 layers in the sol–gel $Cr_{0.11}V_2O_5$ compound, which increases its three-dimensional character and prevents the significant deformations of the framework such as layer puckering, slabs gliding, bonds breaking and polyhedra rotation during electrochemical Li insertion. Further work must be directed towards the study of a similar stability which could be afforded by other trivalent cationic species (Ga^{3+}, $La3^{+}$) incorporated into V_2O_5 via a sol–gel synthesis.

References

[1] M.S. Whittingham, Chem. Rev. 104 (2004) 4271.
[2] R. Baddour, J.P. Pereira-Ramos, R. Messina, J. Perichon, J. Electroanal. Chem. 314 (1991) 81.
[3] S. Passerini, W.H. Smyrl, M. Berrettoni, R. Tossici, M. Rosolen, R. Marassi, F. Decker, Solid State Ionics 90 (1996) 5.
[4] F. Coustier, J.M. Lee, S. Passerini, W.H. Smyrl, Solid State Ionics 116 (1999) 279.
[5] S. Passerini, J.J. Ressler, D.B. Le, B.B. Owens, W.H. Smyrl, Electrochim. Acta 44 (1999) 2209.
[6] Y. Wang, G. Cao, Adv. Mater. 20 (2008) 2251.
[7] C.Q. Feng, S.Y. Wang, R. Zeng, Z.P. Guo, K. Konstantinov, H.K. Liu, J. Power Sources 184 (2008) 485.
[8] S.H. Ng, S.Y. Chew, J. Wang, D. Wexler, Y. Tournayre, K. Konstantinov, H.K. Liu, J. Power Sources 174 (2007) 1032.
[9] M. Inagaki, K. Omori, T. Tsumura, A. Shimizu, Solid State Ionics 86–88 (1996) 849.
[10] M. Inagaki, K. Omori, T. Tsumura, T. Watanabe, A. Shimizu, Solid State Ionics 78 (1995) 275.
[11] V. Vivier, R. Baddour-Hadjean, J.P. Pereira-Ramos, N. Baffier, J. Mater. Chem. 8 (1998) 245.
[12] R. Baddour-Hadjean, J. Farcy, J.P. Pereira-Ramos, N. Baffier, J. Electrochem. Soc. 143 (1996) 2083.
[13] J. Farcy, S. Maingot, P. Soudan, J.P. Pereira-Ramos, N. Baffier, Solid State Ionics 99 (1997) 61.
[14] P. Soudan, J.P. Pereira-Ramos, J. Farcy, G. Grégoire, N. Baffier, Solid State Ionics 135 (2000) 291.
[15] P.G. Dickens, S.J. French, A.T. Hight, M.F. Pye, Mater. Res. Bull. 14 (1979) 1295.
[16] D.W. Murphy, P.A. Christian, F.J. DiSalvo, J.V. Waszczak, Inorg. Chem. 18 (1979) 2800.
[17] C. Delmas, H. Cognac-Auradou, J.M. Cocciantelli, M. Ménétrier, J.P. Doumerc, Solid State Ionics 69 (1994) 257.
[18] J.M. Cocciantelli, J.P. Doumerc, M. Pouchard, M. Broussely, J. Labat, J. Power Sources 34 (1991) 103.
[19] J. Livage, Chem. Rev. 3 (1991) 578.
[20] G. Grégoire, N. Baffier, A. Kahn-Harari, J.C. Badot, J. Mater. Chem. 8 (1998) 2103.
[21] R.J. Cava, A. Santoro, D.W. Murphy, S.M. Zahurak, R.M. Fleming, P. Marsh, R.S. Roth, J. Solid State Chem. 65 (1986) 63.
[22] J.M. Cocciantelli, M. Ménétrier, C. Delmas, J.P. Doumerc, M. Pouchard, P. Hagenmüller, Solid State Ionics 50 (1992) 99.
[23] R. Baddour-Hadjean, E. Raekelboom, J.P. Pereira-Ramos, Chem. Mater. 18 (2006) 3548.
[24] J. Galy, J. Solid State Chem. 100 (1992) 229.
[25] C. Satto, P. Sciau, E. Dooryhee, J. Galy, P. Millet, J. Solid State Chem. 146 (1999) 103.
[26] S.Y. Zhan, C.Z. Wang, K. Nikolowski, H. Ehrenberg, G. Chen, Y.J. Wei, Solid State Ionics 180 (2009) 1198.
[27] R. Baddour-Hadjean, C. Navone, J.P. Pereira-Ramos, Electrochim. Acta 54 (2009) 6674.
[28] R. Baddour-Hadjean, J.P. Pereira-Ramos, C. Navone, M. Smirnov, Chem. Mater. 20 (2008) 1916.
[29] P.G. Bruce, B. Scrosati, J.M. Tarascon, Angew. Chem. Int. Ed. 47 (2008) 2930.
[30] K. West, B. Zachau-Christiansen, T. Jacobsen, S. Skaarup, Solid State Ionics 76 (1995) 15.